## PALEONTOLOGY

# Photosymbiosis and the expansion of shallow-water corals

Katarzyna Frankowiak,[1] Xingchen T. Wang,[2] Daniel M. Sigman,[2] Anne M. Gothmann,[3] Marcelo V. Kitahara,[4] Maciej Mazur,[5] Anders Meibom,[6] Jarosław Stolarski[1]*

Roughly 240 million years ago (Ma), scleractinian corals rapidly expanded and diversified across shallow marine environments. The main driver behind this evolution is uncertain, but the ecological success of modern reef-building corals is attributed to their nutritional symbiosis with photosynthesizing dinoflagellate algae. We show that a suite of exceptionally preserved Late Triassic (ca. 212 Ma) coral skeletons from Antalya (Turkey) have microstructures, carbonate $^{13}C/^{12}C$ and $^{18}O/^{16}O$, and intracrystalline skeletal organic matter $^{15}N/^{14}N$ all indicating symbiosis. This includes species with growth forms conventionally considered asymbiotic. The nitrogen isotopes further suggest that their Tethys Sea habitat was a nutrient-poor, low-productivity marine environment in which photosymbiosis would be highly advantageous. Thus, coral-dinoflagellate symbiosis was likely a key driver in the evolution and expansion of shallow-water scleractinians.

## INTRODUCTION

Symbiosis between scleractinian corals and endocellular dinoflagellate algae (known as zooxanthellae) is key to the success of modern reefs in oligotrophic (sub)tropical waters. The coral host benefits from this association through the translocation of photosynthates and an increased capability to recycle metabolic waste products, such as ammonium (1, 2). The physiological mechanisms and the molecular background underlying this partnership have been extensively studied (2–5). Nevertheless, fundamental questions regarding the coevolution of photosynthesizing algae and corals remain, for example, with regard to the role of photosymbiosis during the sudden Triassic expansion of coral reefs (6). Molecular phylogeny indicates that existing clades of endosymbiotic dinoflagellates originated in the Early Paleogene [that is, only about 60 million years ago (Ma)] (7), and fossil coral skeletons do not preserve direct evidence of the presence of these symbionts. Through comparison with modern corals, indirect criteria, such as macromorphology and isotope geochemistry, have been developed to investigate photosymbiosis in fossil corals (8). For example, most modern symbiotic corals tend to form highly integrated colonies with small (<5 mm) corallites, whereas asymbiotic corals tend to have solitary growth forms or poorly integrated (phaceloid) colonies with larger corallites (9). However, numerous exceptions exist in these morphological traits, pointing to the need for additional, more definitive indicators. Skeletal isotopic compositions have been used to distinguish symbiotic from asymbiotic corals. Modern asymbiotic corals show a wide range of positively correlated $^{18}O/^{16}O$ and $^{13}C/^{12}C$ ratios, whereas these ratios are uncorrelated and have a tendency for higher $^{13}C/^{12}C$ in symbiotic corals (10). In addition, intracrystalline organic matter (OM) in asymbiotic corals has higher $^{15}N/^{14}N$ ratios than intracrystalline OM in symbiotic corals (11). Although these isotopic criteria hold strong potential as proxies for symbiosis in fossil corals,

their application requires exceptional preservation of primary skeleton. This is rare in the fossil record because the aragonite polymorph is unstable under ambient conditions and recrystallizes to calcite, with associated modifications of original skeletal composition.

Recently, two key method developments have created new opportunities for the investigation of photosymbiosis among fossil corals. First, microscale skeletal growth bands have been shown to provide a robust diagnostic signature of photosymbiosis in scleractinian corals (12). Modern symbiotic corals have, almost without exception, highly regular microscale growth bands, whereas these growth bands in asymbiotic corals are irregular and often discontinuous. This difference can be quantified with the coefficient of variation (CV) of bandwidths and thus used as an indicator of photosymbiosis. Skeletons of modern asymbiotic corals are characterized by CVs >40% (Fig. 1B) versus <20% in symbiotic corals. Second, a new "persulfate-denitrifier" method makes high-precision analysis of nitrogen (N) isotopic compositions of intracrystalline OM possible with minute skeleton samples, making it possible to sample only original, unaltered skeletal aragonite (13).

## RESULTS AND DISCUSSION

We applied these new skeleton-based indicators of photosymbiosis to a suite of fossil coral skeletons from the lower Norian outcrops (about 212 Ma) of the Lycian Taurus (near Gödene, Alakir Çay Valley, Antalya Province, Turkey), which provide a unique opportunity to investigate the onset of photosymbiosis among scleractinians (Fig. 1A). Coral colonies occur in "cipit blocks" (reef limestone blocks deposited in slope/basinal sediments) derived from the destruction and redeposition of shallow-water patch reefs that developed during early Norian on the southern part of the Apulia-Taurus platform, along the western margin of the Tethys Ocean (fig. S1) (14). The locality is well known for its excellent preservation of fossil corals (15), which was verified in this study with a broad range of complementary analytical techniques (see the Supplementary Materials). Ultrastructurally, the skeletons consist of two main components: the "rapid accretion deposits" (RADs; also known as centers of calcification) which form a narrow, central zone of septa (ca. 5 volume %), and "thickening deposits" (TDs; also known as fibers) which constitute the main skeletal component (ca. 95 volume %) (16). The RADs are originally nanocrystalline (17, 18) and in comparison to TDs are easily altered during diagenesis. RADs in Triassic corals often

[1]Institute of Paleobiology, Polish Academy of Sciences, Twarda 51/55, PL-00-818 Warsaw, Poland. [2]Department of Geosciences, Princeton University, Princeton, NJ 08544, USA. [3]School of Oceanography, University of Washington, 1492 NE Boat Street, Seattle, WA 98105, USA. [4]Marine Sciences Department, Federal University of São Paulo, Santos, São Paulo 11030-400, Brazil. [5]Department of Chemistry, University of Warsaw, Pasteura 1, PL-02-093 Warsaw, Poland. [6]Laboratory for Biological Geochemistry, School of Architecture, Civil and Environmental Engineering, Ecole Polytechnique Fédérale de Lausanne, and Center for Advanced Surface Analysis, Institute of Earth Sciences, Université de Lausanne, CH-1015 Lausanne, Switzerland.
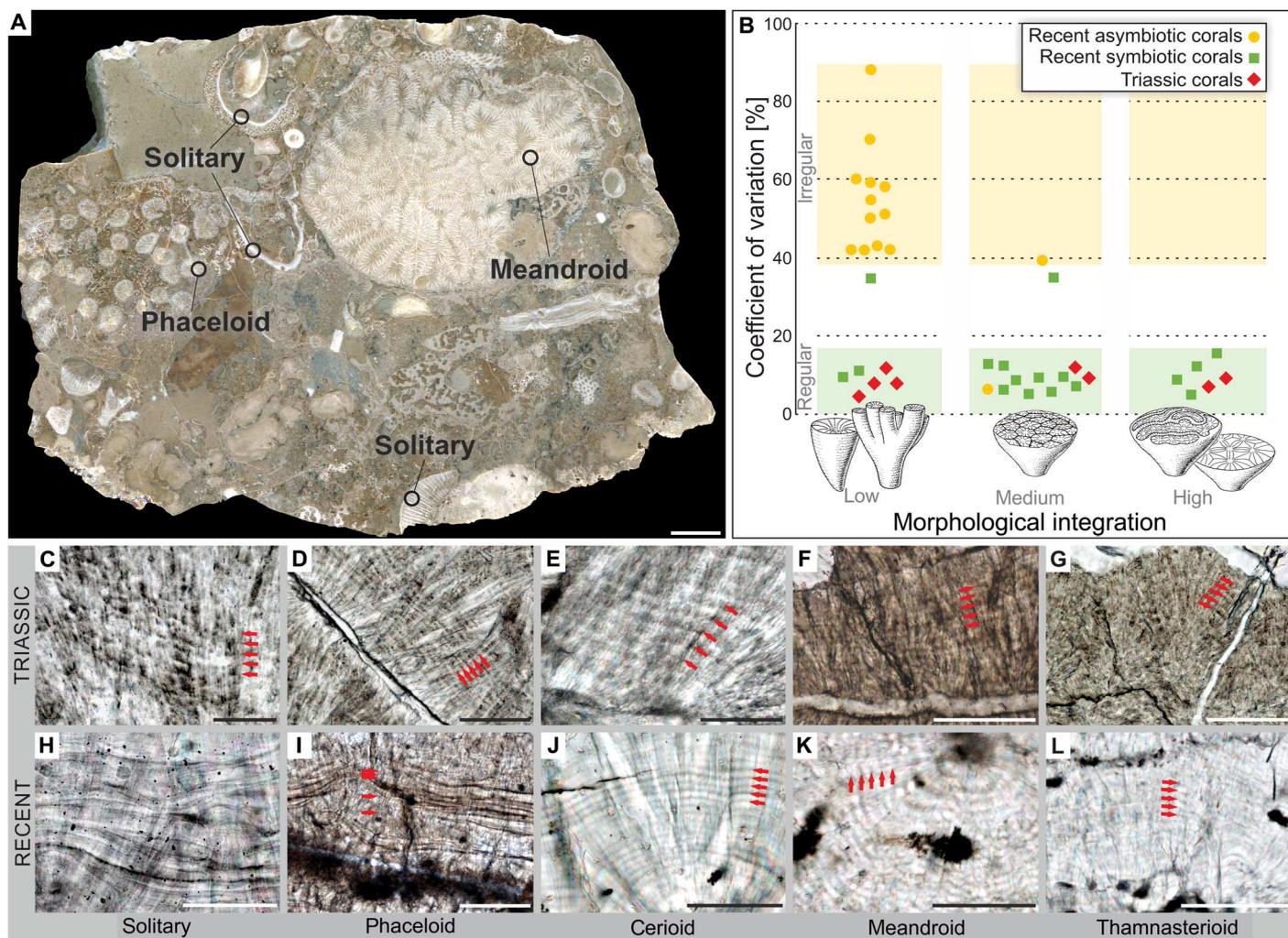*Corresponding author. Email: stolacy@twarda.pan.pl

**Fig. 1. Macrostructural and microstructural characteristics of modern and Triassic corals.** (**A**) Polished slab showing morphological diversity of corals from Antalya (Turkey). (**B**) CV of growth band thickness in modern asymbiotic (yellow dots) and symbiotic (green squares) scleractinian corals. All Triassic corals (red diamonds), irrespective of growth form, show regular growth banding, that is, low CV values, consistent with a symbiotic lifestyle. Growth increments of TDs (transmitted light images) in the Triassic *Coryphyllia* sp. (solitary) (**C**), *Volzeia* aff. *badiotica* (phaceloid) (**D**), *Cerioheterastraea cerioidea* (cerioid) (**E**), *Meandrovolzeia serialis* (meandroid) (**F**), and *Ampakabastraea nodosa* (thamnasterioid) (**G**) in direct comparison with modern corals: asymbiotic *Desmophyllum dianthus* (solitary) (**H**), *Lophelia pertusa* (phaceloid) (**I**), symbiotic *Goniastraea* sp. (cerioid) (**J**), *Symphyllia radians* (meandroid) (**K**), and *Pavona cactus* (thamnasterioid) (**L**). Measurements and taxonomic attribution are provided in tables S1 and S2. Scale bars, 10 mm (A) and 50 μm (C to L).

have crystal textures characteristic of diagenetic calcite spar (fig. S2D), the presence of which was independently confirmed by micro-Raman mapping (green color; fig. S2, E to H). To avoid these regions during geochemical sampling, we characterized their distribution in the skeleton.

In comparison to RADs, TDs are composed of denser aragonite, which is relatively poor in OM. Therefore, these regions better preserved their original structures in fossil corals (*19*). We considered the TDs in the fossil coral skeletons to be well preserved only when meeting all of the following criteria (*19*, *20*): (i) arrangement of crystals and crystal habits identical to those in modern Scleractinia, (ii) absence of Mn-induced luminescence, and (iii) purely aragonitic mineralogy. In addition, areas of well-preserved TDs in a skeleton were required to be large enough to be comfortably sampled with a microdrill (drill bit diameter, 350 μm). Among the 70 fossil coral specimens investigated, 29 met these criteria and were analyzed further (figs. S2, S3, and S4a to 4i, and tables S1 to S3).

In these samples, transmitted light images of TD revealed the presence of centrifugally arranged fibers grouped in bundles (Fig. 1, C to G). Fibers were observed to have doublets of optically light and dark bands representing growth increments (*12*), which are also observable in scanning electron microscopy (SEM) as layers with positive and negative etching relief, respectively (figs. S2D and S3, E and F). These TDs were usually preserved as pure aragonite, as demonstrated by a lack of cathodoluminescence (CL) signal (figs. S2C, S3D, and S4a to S4i) and by Raman spectral imaging (figs. S2, E to H, and S3C). Occasionally, small areas (a few micrometers in size) had been altered to contain minor calcite deposits, which were avoided during sampling for isotopic and structural analysis (see the Supplementary Materials). Care was also taken to avoid skeletal regions with secondary aragonite cements (for example, fig. S4a D, S4h B), which were recognized on some lateral faces of corallite structures (black-colored crystals in CL), as well as calcite infillings of intracorallite spaces (red luminescence in

CL; figs. S4a to S4i). This strict exclusion of secondary phases and altered skeleton structures ensured that only the most pristine skeleton regions were selected.

We compared the microscale banding of the selected Triassic corals to those observed in modern corals, spanning the full spectrum of growth forms from solitary and poorly integrated colonies to highly integrated coralla: solitary (*Coryphyllia* and *Desmophyllum*), phaceloid (*Volzeia* and *Lophelia*), cerioid (*Cerioheterastraea* and *Goniastraea*), meandroid (*Meandrovolzeia* and *Symphyllia*), and thamnasterioid (*Ampakabastraea* and *Pavona*) (Fig. 1, C to L). We found that all selected Triassic corals exhibited highly regular, continuous microscale growth bands that are typical of modern symbiotic corals (table S4). Banding thickness ranged from 3 μm (*Volzeia* aff. *badiotica*) to 10 μm (*Volzeia* sp. A), and growth band CV in each fossil coral was systematically low, between 5 and 12% (Fig. 1B and table S5), indicating that each of the studied Triassic corals harbored photosymbionts.

Muscatine *et al.* (*11*) were the first to use the N isotopes of intracrystalline OM in fossil coral skeleton as a proxy for coral symbiosis. Analytical limitations of this pioneering effort required ~50 g of skeletal material for each analysis, making it impossible to avoid diagenetic calcite during sampling. The new persulfate-denitrifier method allows high-precision isotopic analysis of intracrystalline OM with skeleton samples of only 5 to 10 mg (*13*), allowing targeted sampling of pristine skeleton. The protocol includes rigorous cleaning to remove extraskeletal organic N before isotopic analysis. With this protocol, we observed for the first time a systematic difference in coral skeletal OM $\delta^{15}$N (CS-$\delta^{15}$N) between extant symbiotic and asymbiotic corals exposed to identical environmental conditions; this comparison was conducted off the coast of Ilha dos Búzios, Brazil (Fig. 2A). Here, symbiotic corals exhibited 3 to 4‰ lower CS-$\delta^{15}$N. This difference can be explained as the result of leakage of low-$\delta^{15}$N metabolic waste products from asymbiotic corals, whereas symbiotic corals recycle this N to dinoflagellates (*11*). A recent global study by Wang *et al.* (*21*) showed a systematic CS-$\delta^{15}$N offset of ca. 7‰ between symbiotic and asymbiotic corals (Fig. 2B, see also table S6). The greater amplitude of $\delta^{15}$N difference between asymbiotic and symbiotic corals in the global compilation relative to the Brazilian case study (Fig. 2A) suggests an additional distinction between the symbiotic and asymbiotic corals in the global compilation. The additional distinction is likely that most of the asymbiotic corals were collected from below the euphotic zone, where suspended particulate N has elevated $\delta^{15}$N due to partial decomposition (*22*). Scleractinian corals may harbor nondinoflagellate symbionts, such as nitrogen-fixing cyanobacteria (*23*). However, their influence on coral tissue $\delta^{15}$N (and, consequently, on CS-$\delta^{15}$N) has not been observed to be significant to date (*24*).

Intracrystalline OM in selected Triassic corals from Antalya had a CS-$\delta^{15}$N of ~2 to ~7‰ (shown left of the *y* axis in Fig. 2B), with an average of 3.8 ± 1.3‰ (*n* = 26, 1 SD) (table S3). This range falls below that of modern asymbiotic corals measured to date. If these corals were asymbiotic (that is, plotting along the upper, yellow trend line in Fig. 2B), then their CS-$\delta^{15}$N would suggest that local N sources in the Triassic had a very low $\delta^{15}$N (less than −2‰), which would be inconsistent with the $\delta^{15}$N of Norian marine sediments (*25*). On the other hand, the measured range of CS-$\delta^{15}$N for the Triassic Antalya corals overlaps with the range for modern symbiotic corals, suggesting that all of the measured Triassic corals were symbiotic. If the Triassic corals were symbiotic (that is, plotting along the green trend line in Fig. 2B), then their CS-$\delta^{15}$N would indicate local source $\delta^{15}$N in the range of ~1 to 5‰ with an average around 3‰, similar to the $\delta^{15}$N of nitrate
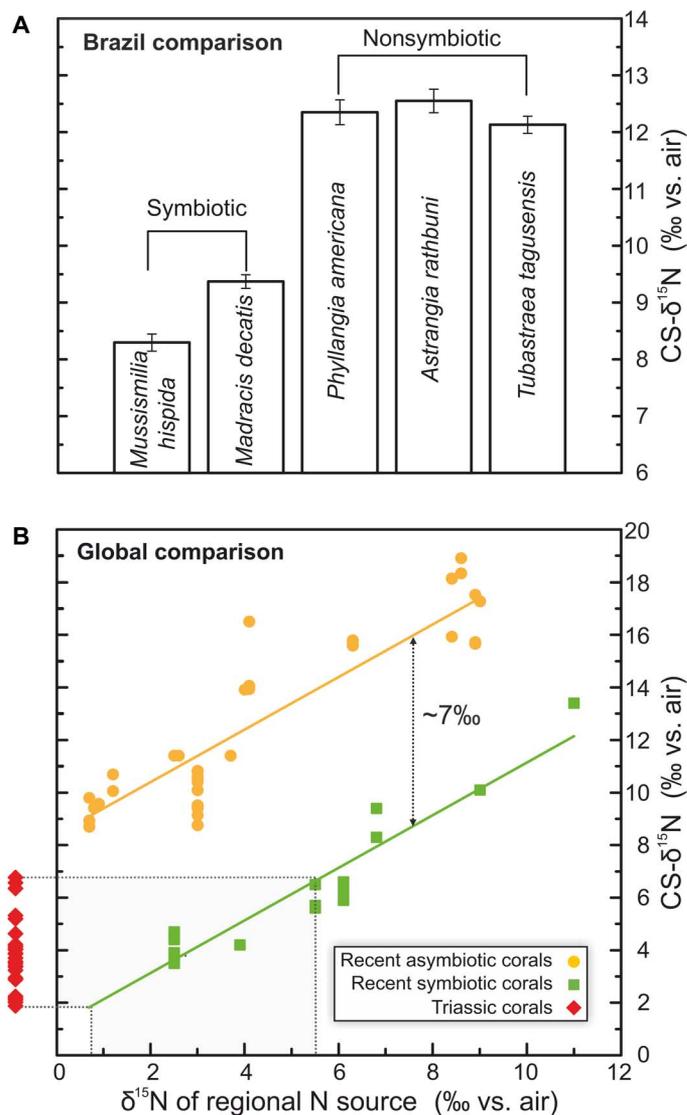


**Fig. 2. Nitrogen isotopic signatures of modern and Triassic corals.** (**A**) Distinction of symbiotic and asymbiotic modern corals based on N isotopic composition of intraskeletal OM (CS-$\delta^{15}$N). All corals were from the same locality (Ilha dos Búzios, Brazil), within an area of ca. 5 m² at a depth of 5 m (table S3). (**B**) Global comparison of CS-$\delta^{15}$N in modern symbiotic and asymbiotic corals correlates with the N isotopic composition of the corresponding local N sources (*22, 23*). The regression equations with fixed 1:1 slope for the modern asymbiotic corals (all deeper than 200 m) and symbiotic corals (all shallower than 20 m) are $Y = X + 8.4‰$ ($R^2 = 0.82$) and $Y = X + 1.1‰$ ($R^2 = 0.88$), respectively. The typical offset between modern symbiotic and asymbiotic corals is ~7‰. The Triassic corals from Antalya have a CS-$\delta^{15}$N range (~2 to ~7‰) that does not overlap with modern asymbiotic corals. Their average CS-$\delta^{15}$N (3.8 ± 1.3‰) is similar to the lowest CS-$\delta^{15}$N measured to date in modern symbiotic corals, which are from offshore Bermuda in the subtropical North Atlantic.

in the modern western tropical and subtropical North Atlantic (*13*). The low $\delta^{15}$N of the nitrate supply in this region is ultimately due to nutrient impoverishment associated with the strong density stratification of tropical waters and the downwelling of subtropical gyres, as well as to the remoteness of this region from the upwelling, higher productivity, and water column denitrification characterizing eastern

ocean basin margins. Nitrogen fixation, which adds N with low $\delta^{15}$N to the upper water column, appears to occur dominantly in low-nutrient tropical and subtropical ocean environments today (26). Moreover, once the biomass produced with newly fixed N sinks into the shallow subsurface and the N is oxidized to nitrate, this low-$\delta^{15}$N nitrate is well isolated by density from the higher-$\delta^{15}$N nitrate in deeper water (27). The net result is that, in the western tropical and subtropical North Atlantic, the $\delta^{15}$N of the nitrate supply to surface ocean biomass is the lowest known in the global ocean (28). Thus, the similarity of the CS-$\delta^{15}$N between the Triassic corals and modern Bermuda corals (Fig. 2B) suggests that the former grew in similarly oligotrophic waters. This oligotrophy might have induced the establishment of photosymbiosis, which would have given these corals an ecological advantage.

Photosynthesis imparts high $\delta^{13}$C on symbiotic coral skeletons, relative to asymbiotic species from similar environments (29). In contrast, skeletal $\delta^{18}$O is not directly affected by photosynthesis but may be related to the rate of coral calcification through kinetic and/or equilibrium isotope effects (29, 30). Together, these factors produce different patterns in skeletal $\delta^{18}$O and $\delta^{13}$C for symbiotic and asymbiotic species (Fig. 3 and fig. S5). The Triassic coral skeletons exhibit carbonate $\delta^{18}$O and $\delta^{13}$C values compatible with modern symbiotic corals (Fig. 3 and tables S2 and S7) but with an offset in $\delta^{13}$C that may be due to a higher $\delta^{13}$C of dissolved inorganic carbon of Triassic seawater (8). Secondary calcite cements from Triassic corals had $\delta^{18}$O and $\delta^{13}$C different from the pure skeleton compositions, tending to plot closer to the field of asymbiotic corals (fig. S6). Potential contamination with secondary calcite, if present despite the strict selection of material for this study, would thus have biased the skeletal compositions toward values for asymbiotic corals. Therefore, measured skeletal $\delta^{13}$C and $\delta^{18}$O also indicated that the Triassic corals studied here were symbiotic (Fig. 3).

In conclusion, the combination of new microstructural criteria, highly sensitive measurements of $^{15}$N/$^{14}$N of OM bound within primary coral aragonite, and C and O isotopic measurements of carefully selected skeleton samples provides a new, powerful toolkit for assessing photosymbiosis in well-preserved fossil corals. Together, these criteria support the interpretation that all Triassic taxa from Turkey examined in this study lived in symbiosis with photosynthesizing dinoflagellate algae. Because most of these coral taxa were widespread on the Late Triassic reefs of the NW Tethys Ocean (31), we propose that symbiosis was the prevailing lifestyle among shallow-water reef-building corals from the Tethyan realm. Surprisingly, this includes small solitary and phaceloid growth forms (such as *Volzeia*, *Pachysolenia*, or *Margarosmilia*) that would have been considered asymbiotic taxa based on classic, macromorphological criteria (9). Shallow-water, low-nutrient marine environments, similar to many modern tropical localities, provided strong impetus for the establishment of this nutritional symbiosis during that time. The algae that became involved in symbiosis with Triassic corals might have been suessiacean dinoflagellates, considered to be the ancestors of modern *Symbiodinium* (2), and their fossilized cysts are known from this period (32, 33). The benefits of this symbiosis, including light-enhanced calcification, allowed corals to acquire a significant position as reef builders. The relative frequency of primary and secondary carbonate frame-building groups in the fossil record shows that the diversity of scleractinian corals increased sharply from Middle Triassic to Late Triassic (31). Since then, the scleractinian coral-dinoflagellate symbiotic relationship has facilitated the formation of widespread coral reefs.

## MATERIALS AND METHODS
The fossil skeletons used in the present study were derived from the lower Norian outcrops of the Lycian Taurus (near Gödene, Alakir Çay Valley, Antalya Province, Turkey). We recognized 9 of about 26 species described from Turkey Triassic localities by Cuif (34–38).
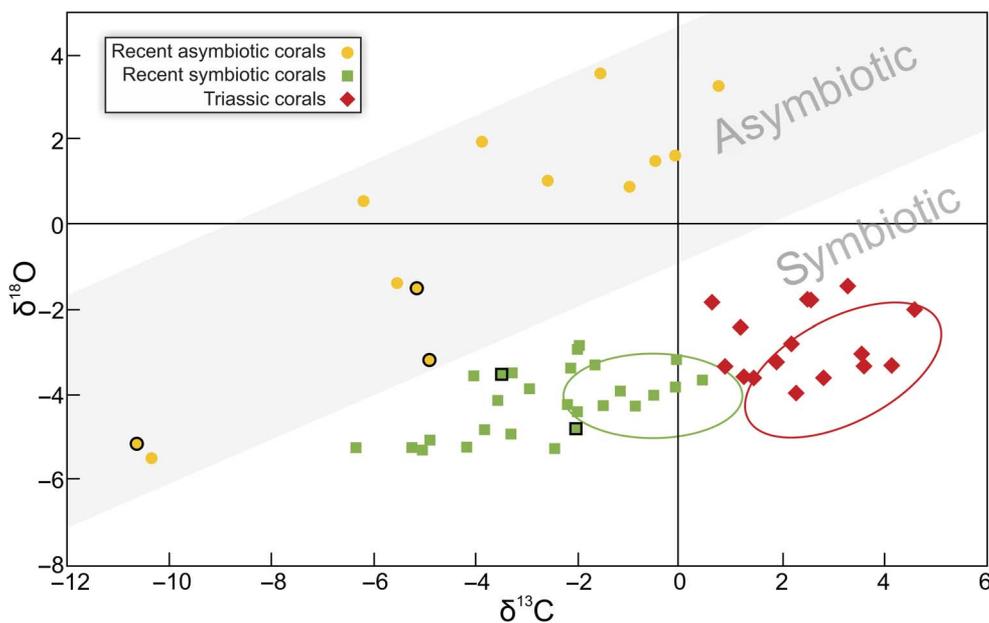
**Fig. 3. Carbon and oxygen isotopic composition of modern and Triassic corals.** Modern asymbiotic corals (yellow dots) plot in a field (grey) distinct from symbiotic corals (green squares) (10) and Triassic corals (this study; red diamonds). Symbiotic and asymbiotic corals from the same locality (Ilha dos Búzios, Brazil) have a black outline. Ellipses show previous measurements of Triassic (red) and modern (green) samples of symbiotic corals (8).

Seven additional species are left in open nomenclature, and six other species are new in this region (that is, *Sichuanophyllia sichuanensis*, *Volzeia* aff. *badiotica*, *Volzeia* aff. *subdichotoma*, *Noriphyllia anatoliensis*, *Margarosmilia capitata*, and *Gablonzeria profunda*). Of 22 taxa, 5 are solitary, 7 are phaceloid, 7 are cerioid, 2 are meandroid, and 1 is thamnasterioid (table S1). On the basis of observations with an optical microscope, we selected the following corals that presented well-defined RADs and TDs, suggesting good skeleton preservation (family-rank taxonomic assignment are given in table S1): *Ampakabastraea nodosa* Cuif, 1976; *Alpinoseris* sp.; *Ceriohetereastraea cerioidea* Cuif, 1976; *Coryphyllia regularis* Cuif, 1974; *Distichiomeadnra spinosa* Cuif, 1976; *Gablonzeria reussi* Cuif, 1976; *G. profunda* Frech, 1890; *Guembelastraea* sp.; *Margarophyllia capitata* Cuif, 1974; *Margarophyllia* sp.; *Margarosmilia* sp.; *Meandrovolzeia serialis* Cuif, 1976; *Noriphyllia anatoliensis* Roniewicz and Stanley, 2009; *Noriphyllia* sp.; *Pachysolenia cylindrica* Cuif, 1975; *Pachythecalis major* Cuif, 1975; *Volzeia* sp. A; *Retiophyllia* type IV Cuif, 1974; *Retiophyllia* sp.; *Sichuanophyllia sichuanensis* Deng-Zhanqiu and Zhang-Yansheng, 1984; *Toechastraea* sp.; *Volzeia* aff. badiotica Volz, 1896; and *V.* aff. subdichiotoma Münster, 1841. Our Triassic material included six (of eight) genera analyzed previously by Stanley and Swart (*8*) (that is, *Pachythecalis*, *Pachysolenia*, *Guembelastraea*, *Toechastraea*, *Retiophyllia*, and *Coryphyllia*), whereas six genera are new (that is, *Sichuanophyllia*, *Volzeia*, *Noriphyllia*, *Margarophyllia*, *Ceriohetereastraea*, and *Gablonzeria*). We also studied a set of modern symbiotic and asymbiotic corals, collected from different shallow-water and deepwater sites (details are in tables S2, S4, and S6), for comparison with our fossil samples. Thin sections of all specimens were, and are currently, housed at the Institute of Paleobiology, Polish Academy of Sciences, Warsaw (ZPAL).

Reliable interpretation of geochemical signatures from fossil samples requires rigorous testing against traces of diagenetic alteration of the skeleton. The microscopic and spectroscopic techniques used for diagenetic testing are listed below. Brief descriptions of oxygen, carbon, and nitrogen stable isotope measurements follow.

## Optical microscopy
Polished sections were examined using a Nikon Eclipse 80i transmitted light microscope fitted with a DS-5Mc cooled camera head, at the ZPAL. Observations were conducted in transmitted light, which allowed for a quick assessment of the fossil's microstructural organization. Microstructures comparable to those of modern scleractinians potentially contain primary material. Microstructures different from modern scleractinians were classified as diagenetically altered (for example, those that consist of large crystals of sparry calcite, indicating recrystallization).

## Scanning electron microscopy
Polished sections were etched for 10 s in 0.1% formic acid, rinsed with Milli-Q water, and air-dried. Next, the specimens were placed on stubs with double sticky tape and sputter-coated with conductive platinum film. Analyses were made using a Phillips XL20 scanning electron microscope at the ZPAL. SEM imaging provided high-resolution support of transmitted light observations. For example, SEM studies made it possible to obtain more detailed information about crystal textures to better distinguish fibrous aragonite from sparry calcite.

## CL microscopy
Fossil corals were analyzed using CL microscopy. Thin sections of corallites cross-sectioned in the transverse plane were polished and coated with carbon. CL analysis was performed using a hot cathode microscope, HC1-LM, at the ZPAL, with the following parameters: an electron energy of 14 keV and a beam current density of 0.1 $\mu$A mm$^{-2}$. CL is a simple method to determine the spatial distribution of primary (aragonite) and secondary (calcite) features in coral skeleton (*20*). Diagenetic calcite typically contains a high concentration of Mn$^{2+}$ [the main activator of luminescence in carbonates (*39*)] and exhibits strong orange-to-red luminescence. In contrast, in original skeletal aragonite, the abundance of Mn is much lower than that in diagenetic calcite, especially because of (i) a higher partition coefficient for Mn in calcite than in aragonite and (ii) higher concentrations of Mn in the reducing waters (relative to seawater) from which secondary cements are often formed.

## Raman microscopy
Raman confocal microscopy was used to achieve a better spatial understanding of calcite and aragonite distributions in the Triassic samples, as well as to verify CL microscopy observations. Briefly, Raman maps were recorded at integration times of 1 or 5 s with a spatial resolution of 1 $\mu$m × 1 $\mu$m using a LabRAM HR 800 Raman confocal microscope (Horiba Jobin Yvon) equipped with an LPF Iridia edge filter, a 600 or 1800 groove mm$^{-1}$ holographic grating, and a 1024-pixel × 256-pixel Peltier-cooled Synapse charge-coupled device detector. The microscope attachment was based on an Olympus BX41 system with an MPLN 100× objective and a motorized software-controlled *x-y-z* stage. The excitation source was the second harmonic of the diode-pumped neodymium-doped yttrium aluminum garnet laser (Excelsior-532-100, Spectra-Physics) operating at 532.3 nm with ca. 2-mW power on the sample. The most convenient signals allowing for the identification of the calcite and aragonite polymorphs were grouped in the 100 to 300 cm$^{-1}$ region. These peaks, associated with lattice vibrations, appeared at 205 and 153 cm$^{-1}$ for aragonite. For calcite, the bands could be found at 281 and 153 cm$^{-1}$. To visualize distribution of calcite and aragonite in the samples, the ratio of the intensities at 281 and 205 cm$^{-1}$ was calculated (the maps were processed with LabSpec 5, Horiba Jobin Yvon software). The high values of the ratio corresponded to the high abundance of calcite in the sample (in green), whereas the low value of the ratio indicated high content of aragonite (in blue). Analyses were performed at the Department of Chemistry, University of Warsaw.

## Oxygen and carbon isotopes
The coral carbonate powders were prepared for isotopic analysis according to established procedures (*40*). Next, samples (minimum, 20 $\mu$g) were treated with 100% orthophosphoric acid under vacuum at 70°C in a Thermo Kiel IV Carbonate Device coupled with a Finnigan Delta Plus mass spectrometer. Isotope ratios were reported in per mil (‰) $\delta$ notation relative to the Vienna Pee Dee Belemnite (VPDB) standard (defined via NBS 19). The spectrometer external error was ±0.03‰ for $\delta^{13}$C and ±0.07‰ for $\delta^{18}$O. Analyses were performed at the Institute of Geological Sciences, Polish Academy of Sciences. Oxygen and carbon isotopic compositions were also measured on carbonate infillings (cements) of the Triassic corallites. Sample preparation for infilling cements was the same as described above for primary coral, but the isotopic measurements were conducted using a Sercon Isotope Ratio Mass Spectrometer coupled with a Thermo GasBench II sampling device at Princeton University. Results were calibrated relative to the VPDB standard (defined via NBS 19). Precision of the measurements was ±0.1‰ for $\delta^{13}$C and ±0.2‰ for $\delta^{18}$O.

## Nitrogen isotopes

The $\delta^{15}N$ of skeleton-bound OM was measured at Princeton University following the protocol detailed in the study by Wang *et al.* (13). Briefly, 10 to 20 mg of coral skeleton powder was soaked in concentrated sodium hypochlorite for 24 hours to remove any external N contamination. Then, the skeleton powder was dissolved with HCl, and the released OM was oxidized into nitrate with alkaline persulfate oxidizing reagent. The concentration of the nitrate in the examined sample was analyzed by chemiluminescence (41), whereas $\delta^{15}N$ of nitrate was measured by conversion into nitrous dioxide with the "denitrifier method" (42), followed by automated extraction, purification, and isotopic analysis of the $N_2O$ product (43). Two amino acid reference materials (USGS40 and USGS41) were included in each batch of analyses to correct for the reagent blank of the protocol and to reference the data to atmospheric $N_2$, the universal reference. An in-house coral standard (CBS-I) was also included to monitor the performance of the full method and to characterize long-term precision. The analytical precision of the protocol was 0.2‰.

## SUPPLEMENTARY MATERIALS

Supplementary material for this article is available at http://advances.sciencemag.org/cgi/content/full/2/11/e1601122/DC1

fig. S1. Geology and paleogeography of the Triassic reef deposits.
fig. S2. Microstructural and mineralogical features of the skeleton of the Triassic (early Norian) *Volzeia* sp. A from Alakir Çay, Turkey (ZPAL H.21.27) and modern symbiotic coral *Symphyllia radians*.
fig. S3. Microstructural and mineralogical features of the skeleton of the Triassic (early Norian) cerioid *Cerioheterastraea cerioidea* from Alakir Çay, Turkey (ZPAL H.21.20).
fig. S4a. State of preservation of early Norian solitary scleractinian corals (Alakir Çay, Turkey) used for geochemical analyses.
fig. S4b. State of preservation of early Norian solitary scleractinian corals (Alakir Çay, Turkey) used for geochemical analyses.
fig. S4c. State of preservation early Norian phaceloid scleractinian corals (Alakir Çay, Turkey) used for geochemical analyses.
fig. S4d. State of preservation of early Norian phaceloid scleractinian corals (Alakir Çay, Turkey) used for geochemical analyses.
fig. S4e. State of preservation of early Norian solitary and phaceloid scleractinian corals (Alakir Çay, Turkey) used for geochemical analyses.
fig. S4f. State of preservation of early Norian phaceloid and meandroid scleractinian corals (Alakir Çay, Turkey) used for geochemical analyses.
fig. S4g. State of preservation of early Norian cerioid scleractinian corals (Alakir Çay, Turkey) used for geochemical analyses.
fig. S4h. State of preservation of early Norian cerioid scleractinian corals (Alakir Çay, Turkey) used for geochemical analyses.
fig. S4i. State of preservation of early Norian thick-walled, pachythecaliine corals (Alakir Çay, Turkey) used for geochemical analyses.
fig. S5. Oxygen and carbon isotopic composition of modern symbiotic and asymbiotic corals.
fig. S6. Carbon ($\delta^{13}C$) and oxygen ($\delta^{18}O$) isotopic composition of Triassic corals (Alakir Çay, Turkey) and calcite cements infilling their corallites.
table S1. Inventory numbers, taxonomic attribution, and growth forms of examined Triassic coral samples from Antalya, Turkey.
table S2. Inventory numbers, taxonomic attribution, and oxygen and carbon isotopic composition of Triassic corals from Antalya, Turkey and calcite cement from corresponding corallite infilling (the same inventory number as coral sample but with "_C" ending).
table S3. Nitrogen isotopic composition of OM extracted from Triassic corals from Antalya, Turkey.
table S4. Inventory numbers of sections, taxonomic attribution, locality data, symbiotic status (s, symbiotic; as, asymbiotic), and regularity of growth increments [expressed as CV (%) of dispersion of values of band thickness obtained from each skeleton] of examined modern scleractinian coral samples.
table S5. Inventory numbers of sections (including numbers in Fig. 1), taxonomic attribution, and regularity of growth increments [expressed as CV (%) of dispersion of values of band thickness obtained from each skeleton] of examined fossil (Triassic) corals from Alakir Çay, Turkey.
table S6. Nitrogen isotopic composition of skeleton-bound OM from modern symbiotic and asymbiotic corals.

table S7. Inventory numbers of sections, taxonomic attribution, locality data, symbiotic status (s, symbiotic; as, asymbiotic), and oxygen and carbon isotopic composition of modern symbiotic and asymbiotic corals.
References (44–51)

## REFERENCES AND NOTES

1. C. M. Yonge, A. G. Nicholls, Studies on the physiology of corals. V. On the relationship between corals and zooxanthellae. *Sci. Rep. Gr. Barrier Reef Exped.* **1**, 177–211 (1931).
2. S. K. Davy, D. Allemand, V. M. Weis, Cell biology of cnidarian-dinoflagellate symbiosis. *Microbiol. Mol. Biol. Rev.* **76**, 229–261 (2012).
3. V. M. Weis, S. K. Davy, O. Hoegh-Guldberg, M. Rodriguez-Lanetty, J. R. Pringle, Cell biology in model systems as the key to understanding corals. *Trends Ecol. Evol.* **23**, 369–376 (2008).
4. C. Kopp, M. Pernice, I. Domart-Coulon, C. Djediat, J. E. Spangenberg, D. T. L. Alexander, M. Hignette, T. Meziane, A. Meibom, Highly dynamic cellular-level response of symbiotic coral to a sudden increase in environmental nitrogen. *mBio* **4**, e00052-e13 (2013).
5. C. Kopp, I. Domart-Coulon, S. Escrig, B. M. Humbel, M. Hignette, A. Meibom, Subcellular investigation of photosynthesis-driven carbon assimilation in the symbiotic reef coral *Pocillopora damicornis*. *mBio* **6**, e02299-14 (2015).
6. G. D. Stanley Jr., The evolution of modern corals and their early history. *Earth-Sci. Rev.* **60**, 195–225 (2003).
7. Y. Shaked, C. de Vargas, Pelagic photosymbiosis: rDNA assessment of diversity and evolution of dinoflagellate symbionts and planktonic foraminiferal hosts. *Mar. Ecol. Prog. Ser.* **325**, 59–71 (2006).
8. G. D. Stanley, P. K. Swart, Evolution of the coral-zooxanthellae symbiosis during the Triassic: A geochemical approach. *Paleobiology* **21**, 179–199 (1995).
9. A. G. Coates, J. B. C. Jackson, Clonal growth, algal symbiosis, and reef formation by corals. *Paleobiology* **13**, 363–378 (1987).
10. P. K. Swart, Carbon and oxygen isotope fractionation in scleractinian corals: A review. *Earth-Sci. Rev.* **19**, 51–80 (1983).
11. L. Muscatine, C. Goiran, L. Land, J. Jaubert, J.-P. Cuif, D. Allemand, Stable isotopes ($\delta^{13}C$ and $\delta^{15}N$) of organic matrix from coral skeleton. *Proc. Natl. Acad. Sci. U.S.A.* **102**, 1525–1530 (2005).
12. K. Frankowiak, S. Kret, M. Mazur, A. Meibom, M. V. Kitahara, J. Stolarski, Fine-scale skeletal banding can distinguish symbiotic from asymbiotic species among modern and fossil scleractinian corals. *PLOS ONE* **11**, e0147066 (2016).
13. X. T. Wang, D. M. Sigman, A. L. Cohen, D. J. Sinclair, R. M. Sherrell, M. A. Weigand, D. V. Erler, H. Ren, Isotopic composition of skeleton-bound organic nitrogen in reef-building symbiotic corals: A new method and proxy evaluation at Bermuda. *Geochim. Cosmochim. Acta* **148**, 179–190 (2015).
14. E. Flügel, W. Kiessling, *Triassic reef patterns*, in *Phanerozoic Reef Patterns*, W. Kiessling, E. Flügel, J. Golonka, Eds. (SEPM Special Publication, 2002), pp. 391–463.
15. J. P. Cuif, J. C. Fischer, J. Marcoux, Découverte d'une faune de Chaetetida (Cnidaria, Hydrozoa) dans le Trias supérieur de Turquies. *C. R. Acad. Sci. Hebd. Seances Acad. Sci. D* **275**, 185–188 (1972).
16. J. Stolarski, Three-dimensional micro- and nanostructural characteristics of the scleractinian coral skeleton: A biocalcification proxy. *Acta Palaeontol. Pol.* **48**, 497–530 (2003).
17. J.-P. Cuif, Y. Dauphin, Microstructural and physico-chemical characterization of 'centers of calcification' in septa of some Recent scleractinian corals. *Paläont. Z.* **72**, 257–269 (1998).
18. K. Benzerara, N. Menguya, M. Obstb, J. Stolarski, M. Mazur, T. Tylisczak, G. E. Brown Jr., A. Meibom, Study of the crystallographic architecture of corals at the nanoscale by scanning transmission X-ray microscopy and transmission electron microscopy. *Ultramicroscopy* **111**, 1268–1275 (2011).
19. K. Frankowiak, M. Mazur, A. M. Gothmann, J. Stolarski, Diagenetic alteration of Triassic coral from the aragonite Konservat-Lagerstätte in Alakir Çay, Turkey: Implications for geochemical measurements. *Palaios* **28**, 333–342 (2013).
20. A. M. Gothmann, J. Stolarski, J. F. Adkins, B. Schoene, K. J. Dennis, D. P. Schrag, M. Mazur, M. L. Bender, Fossil corals as an archive of secular variations in seawater chemistry since the Mesozoic. *Geochim. Cosmochim. Acta* **160**, 188–208 (2015).
21. X. T. Wang, D. M. Sigman, A. L. Cohen, D. J. Sinclair, R. M. Sherell, K. M. Cobb, D. V. Erler, A. Alpert, J. Stolarski, M. V. Kitahara, H. Ren, Influence of open ocean nitrogen supply on the skeletal $\delta^{15}N$ of modern shallow-water scleractinian corals. *Earth Planet. Sci. Lett.* **441**, 125–132 (2016).
22. X. T. Wang, M. G. Prokopenko, D. M. Sigman, J. F. Adkins, L. F. Robinson, H. Ren, S. Oleynik, B. Williams, G. H. Haug, Isotopic composition of carbonate-bound organic nitrogen in deep-sea scleractinian corals: A new window into past biogeochemical change. *Earth Planet. Sci. Lett.* **400**, 243–250 (2014).

23. M. P. Lesser, C. H. Mazel, M. Y. Gorbunov, P. G. Falkowski, Discovery of symbiotic nitrogen-fixing cyanobacteria in corals. *Science* **305**, 997–1000 (2004).

24. M. P. Lesser, L. I. Falcón, A. Rodríguez-Román, S. Enríquez, O. Hoegh-Guldberg, R. Iglesias-Prieto, Nitrogen fixation by symbiotic cyanobacteria provides a source of nitrogen for the scleractinian coral *Montastraea cavernosa*. *Mar. Ecol. Prog. Ser.* **346**, 143–152 (2007).

25. T. J. Algeo, P. A. Meyers, R. S. Robinson, H. Rowe, G. Q. Jiang, Icehouse–Greenhouse variations in marine denitrification. *Biogeosciences* **11**, 1273–1295 (2014).

26. D. Karl, A. Michaels, B. Bergman, D. Capone, E. Carpenter, R. Letelier, F. Lipschultz, H. Paerl, D. Sigman, L. Stal, Dinitrogen fixation in the world's oceans, in *The Nitrogen Cycle at Regional to Global Scales*, E. Boyer, R. Howarth, Eds. (Springer, 2002), pp. 47–98.

27. D. Marconi, M. A. Weigand, P. A. Rafter, M. R. McIlvin, M. Forbes, K. L. Casciotti, D. M. Sigman, Nitrate isotope distributions on the US GEOTRACES North Atlantic cross-basin section: Signals of polar nitrate sources and low latitude nitrogen cycling. *Mar. Chem.* **177**, 143–156 (2015).

28. D. M. Sigman, P. J. DiFiore, M. P. Hain, C. Deutsch, Y. Wang, D. M. Karl, A. N. Knapp, M. F. Lehman, S. Pantoja, The dual isotopes of deep nitrate as a constraint on the cycle and budget of oceanic fixed nitrogen. *Deep Sea Res. Part I* **56**, 1419–1439 (2009).

29. P. K. Swart, J. J. Leder, The utility of the stable isotopic signature in coral skeletons. *Paleont. Soc. Pap.* **1**, 249–291 (1996).

30. J. F. Adkins, E. A. Boyle, W. B. Curry, A. Lutringer, Stable isotopes in deep-sea corals and a new mechanism for "vital effects". *Geochim. Cosmochim. Acta* **67**, 1129–1143 (2003).

31. P. Riedel, Korallen in der Trias der Tethys: Stratigraphische reichweiten, Diversitätsmuster, entwicklungstrends und Bedeutung als Rifforganismen. *Mitt. Geol. Bergbaustud. Oesterr.* **37**, 97–118 (1991).

32. J. M. Moldowan, J. Dahl, S. R. Jacobson, B. J. Huizinga, F. J. Fago, R. Shetty, D. S. Watt, K. E. Peters, Chemostratigraphic reconstruction of biofacies: Molecular evidence linking cyst-forming dinoflagellates with pre-Triassic ancestors. *Geology* **24**, 159–162 (1996).

33. R. B. Palliani, J. B. Riding, Subdivision of the dinoflagellate cyst family Suessiaceae and discussion of its evolution. *J. Micropalaeontology* **19**, 133–137 (2000).

34. J. P. Cuif, Recherches sur les Madréporaires du Trias. I. Famille Stylophyllidae. *Bull. Mus. Natl. Hist. Nat. Sci. Terre.* **17** (1972), 211–291 (1973).

35. J. P. Cuif, Recherches sur les Madréporaires du Trias. II. Astraeoida. Révision des genres *Montlivaltia* et *Thecosmilia*. Etude de quelques types structuraux du Trias de Turquie. *Bull. Mus. Natl. Hist. Nat. Sci. Terre.* **40** (1974), 293–400 (1975a).

36. J. P. Cuif, Recherches sur les Madréporaires du Trias. III. Études des structures pennulaires chez les Madreporaires triasiques. *Bull. Mus. Natl. Hist. Nat.* **310**, 45–127 (1975).

37. J.-P. Cuif, Caractères morphologiques, microstructuraux et systématiques des *Pachythecalidae* nouvelle famille de Madréporaires triasiques. *Geophys. J. Roy. Astron. Soc.* **8**, 157–180 (1975).

38. J. P. Cuif, Recherches sur les Madréporaires du Trias. Formes cério-méandroides et thamnastérioides du Trias des Alpes et du Taurus sud-anatolien. *Bull. Mus. Natl. Hist. Nat. Sci. Terre.* **53**, 65–195 (1976).

39. D.J. Marshall, *Cathodoluminescence of Geological Materials* (Unwin Hyman Publishing, 1988), pp. 1–243.

40. J. M. McCrea, The isotopic chemistry of carbonates and a paleo-temperature scale. *J. Chem. Phys.* **18**, 849–857 (1950).

41. R. S. Braman, S. A. Hendrix, Nanogram nitrite and nitrate determination in environmental and biological materials by vanadium (III) reduction with chemiluminescence detection. *Anal. Chem.* **61**, 2715–2718 (1989).

42. D. M. Sigman, K. L. Casciotti, M. Andreani, C. Barford, M. Galanter, J. K. Böhlke, A bacterial method for the nitrogen isotopic analysis of nitrate in seawater and freshwater. *Anal. Chem.* **73**, 4145–4153 (2001).

43. M. A. Weigand, J. Foriel, B. Barnett, S. Oleynik, D.M. Sigma, Updates to instrumentation and protocols for isotopic analysis of nitrate by the denitrifier method. *Rapid Commun. Mass Spectrom.* **30**, 1365–1383 (2016).

44. W. Kiessling, E. Flügel, J. Golonka, Paleo reef maps: Evaluation of a comprehensive database on Phanerozoic reefs. *AAPG Bull.* **83**, 1552–1587 (1999).

45. P. Riedel. Riffbiotope im Karn und Nor (Obertrias) der Tethys: Entwicklung, Einschnitte und Diversitätsmuster. 1–96. Unpublished thesis, Universität Erlangen-Nürnberg, Erlangen (1990).

46. M. Delaune-Mayere, J. Marcoux, J.-F. Parrot, A. Poisson, Modele d'évolution Mésozoique de la paléomarge Téthysienne au niveau des nappes radiolaritiques et ophiolitiques du Taurus Lycien, d'Antalya et du Baer-Bassit, in *Structural History of the Mediterranean Basins*, B. Biju-Duval, L. Montadert, Eds. (Technip, 1977), pp. 79–94.

47. M. Gutnic, O. Monod, A. Poisson, J. F. Dumont, Géologie des Taurides occidentales (Turquie). *Mém. Soc. Géol. Fr.* **137**, 109 (1979).

48. J. Marcoux, Antalya Naplarmm Genel Yapısı ve Tetis Güney Kenan Paleocoğrafyasmdaki Yeri. *Türkiye Jeoloji Kurumu Bülteni* **22**, 1–5 (1979).

49. A. H. F. Robertson, N. H. Woodcock, Alakir çay Group, antalya complex, SW Turkey: A deformed Mesozoic carbonate margin. *Sediment. Geol.* **30**, 95–131 (1981).

50. J. Marcoux, A. Baud, L. Krystyn, O. Monod, *Late Permian and Triassic in Western Turkey. Field Workshop 1986, Guide Book Part 2, 4–17* (Subcommission on Triassic stratigraphy, Instanbul Technical Univ., 1986).

51. E. Flügel, M. Link, Upper Triassic reefs of Southwestern Turkey: Evidence of reef boulders ("Cipits"), in *Global and Regional Controls in Biogenic Sedimentation. I. Reef Evolution*, J. Reitner, F. Neuweiler, F. Gunkel, Eds. (Göttinger Arbeiten zur Geologie und Paläontologie Sb2, 1996), pp. 279–283.

# Science Advances

## Photosymbiosis and the expansion of shallow-water corals

Katarzyna Frankowiak, Xingchen T. Wang, Daniel M. Sigman, Anne M. Gothmann, Marcelo V. Kitahara, Maciej Mazur, Anders Meibom and Jaroslaw Stolarski

| | |
|---|---|
| **ARTICLE TOOLS** | http://advances.sciencemag.org/content/2/11/e1601122 |
| **SUPPLEMENTARY MATERIALS** | http://advances.sciencemag.org/content/suppl/2016/10/31/2.11.e1601122.DC1 |
| **REFERENCES** | This article cites 44 articles, 9 of which you can access for free http://advances.sciencemag.org/content/2/11/e1601122#BIBL |
| **PERMISSIONS** | http://www.sciencemag.org/help/reprints-and-permissions |

Use of this article is subject to the Terms of Service